Gutiérrez-Ariza *et al.*
Progress in Earth and Planetary Science (2024) 11:11
https://doi.org/10.1186/s40645-023-00603-w

Progress in Earth and Planetary Science

RESEARCH ARTICLE

Open Access

Magnesium silicate chimneys at the Strytan hydrothermal field, Iceland, as analogues for prebiotic chemistry at alkaline submarine hydrothermal vents on the early Earth

Carlos Gutiérrez-Ariza[1], Laura M. Barge[2], Yang Ding[3], Silvana S. S. Cardoso[3], Shawn Erin McGlynn[4,5], Ryuhei Nakamura[4,5], Donato Giovanelli[4,6], Roy Price[7], Hye Eun Lee[4], F. Javier Huertas[1], C. Ignacio Sainz-Díaz[1] and Julyan H. E. Cartwright[1,8*]

Abstract

The Strytan Hydrothermal Field (SHF) in basaltic terrain in Iceland is one of the extant alkaline submarine hydrothermal vent systems favoured as analogues for where life on Earth may have begun. To test this hypothesis we analyse the composition, structure, and mineralogy of samples from hydrothermal chimneys generated at the SHF. We find that the chimney precipitates are composed of Mg-silicates including clays of the saponite-stevensite group (high Mg and Si, low Fe and Al), Ca-carbonates and Ca-sulfates. The chimneys comprise permeable structures with pores sizes down to 1 μm or less. Their complex interiors as observed with SEM (Scanning Electron Microscopy) and X-ray CT (computed tomography scanning), exhibit high internal surface areas. EDX (energy-dispersive X-ray spectroscopy) analysis reveals an increase in the Mg/Si ratio toward the chimney exteriors. Chemical garden analogue experiments produce similar Mg–silicate chimneys with porous internal structures, indicating that injection-precipitation experiments can be high-fidelity analogues for natural hydrothermal chimneys at the SHF. We conclude that SHF chimneys could have facilitated prebiotic reactions comparable to those proposed for clays and silica gels at putative Hadean to Eoarchean alkaline vents. Analysis of the fluid dynamics shows that these chimneys are intermediate in growth rate compared to faster black smokers though slower than those at Lost City. The SHF is proposed as a prebiotic alkaline vent analogue for basaltic terrains on the early Earth.

Keywords Alkaline submarine hydrothermal vents, Strytan hydrothermal field, Prebiotic chemistry, Origin of life

*Correspondence:
Julyan H. E. Cartwright
julyan.cartwright@csic.es
[1] Instituto Andaluz de Ciencias de la Tierra, CSIC–UGR, 18100 Armilla, Granada, Spain
[2] NASA Jet Propulsion Laboratory, California Institute of Technology, Pasadena, CA, USA
[3] Department of Chemical Engineering and Biotechnology, Cambridge University, Cambridge CB3 0AS, UK
[4] Earth-Life Science Institute, Tokyo Institute of Technology, 2-12-1 Ookayama, Meguro-ku, Tokyo 152-8550, Japan
[5] Center for Sustainable Resource Science, RIKEN, 2-1 Hirosawa, Wako, Saitama 351-0198, Japan
[6] Department of Biology, University of Naples "Federico II", Monte Sant'Angelo, Edificio 7, Stanza 1D-22, 80126 Naples, Italy
[7] School of Marine and Atmospheric Sciences, Stony Brook University, Stony Brook, NY 11794-5000, USA
[8] Instituto Carlos I de Física Teórica y Computacional, Universidad de Granada, 18071 Granada, Spain

1 Introduction

Across the ocean floor one finds hydrothermal vents emitting mineral-laden waters of higher temperature and different pH and composition than ambient seawater. Owing to the differences in concentration, pH, and temperature, minerals are deposited at these vents, where solid chimney structures are formed that reach many metres in height. The composition and timescale of hydrothermal chimney formation varies greatly between different types of vents, whose geochemical characteristics are a result of the host rock type and the degree of magmatic input. On Earth today, vents range from acidic, ~ 300–400 °C "black smokers" with metal-sulfide rich chimneys; intermediate temperature (around 100–300 °C) acidic "white smokers" (Gamo et al. 2004; Kormas et al. 2006; Fustec et al. 1987); and lower-temperature (less than 100 °C) vents with chimneys of brucite and carbonates formed via serpentinization that can range from seawater pH to very alkaline (Okumura et al. 2016a, b; Kelley et al. 2005; Ludwig et al. 2006; Lecoeuvre et al. 2021; Monnin et al. 2014; 2021). These serpentinization-hosted vents generate hydrogen from hydration of olivine, providing energy to support microbial life (Proskurowski et al. 2008; Kelley et al. 2005).

The Lost City Hydrothermal Field (LCHF) in the north Atlantic Ocean was the first discovered serpentinite-hosted deep-sea vent, and its properties have formed the basis for a detailed emergence-of-life theory (Russell and Hall 1997, 2006; Martin et al. 2008) based on the LCHF redox, pH, and chemical gradients that mimic the gradients that life harnesses across cellular membranes (Lane and Martin 2012). It has been proposed that in an early Earth context, a LCHF-like hydrothermal chimney composed of Fe(II)-bearing hydroxides/sulfides/carbonates (due to the anoxic, Fe^{2+}-rich early oceans; MacLeod et al. 1994; Jiang and Tosca 2019; Tosca et al. 2016; Halevy et al. 2017) could have driven prebiotic reactions such as CO_2 reduction and amino acid synthesis toward the emergence of life (Russell and Hall 2006; Russell 2018). The first precipitate in LCHF chimneys is brucite, $Mg(OH)_2$, when alkaline vent fluids react with Mg^{2+} in seawater. Simultaneously, dissolved Ca^{2+} in vent fluids can mix with HCO_3^- in seawater to precipitate calcium carbonate (Früh-Green et al. 2003); in an early Earth ocean the first precipitate at a similar vent would therefore be ferrobrucite and/or green rust (Russell 2018). Green rust—a double layered Fe(II)/Fe(III)-hydroxide—is a mineral of great interest in environmental science and wastewater treatment due to its versatile adsorption capacity and reactivity; e.g., it absorbs phosphorus, and drives abiotic nitrogen redox cycling through reduction of nitrate/nitrite (Hansen et al 2001; Barthélémy et al. 2012; Etique et al. 2014). The presence of green rust in prebiotic alkaline vent chimneys is central to this origin-of-life theory; since green rust is proposed to function as a "nano-engine" driving synthesis of amino acids/peptides/proto-enzymes capable of harnessing hydrothermal pH and redox gradients toward the emergence of autotrophic metabolism (Russell 2018, 2023).

However, it is still unclear what the properties of early Earth seafloor and ocean crust were and thus what the geochemical characteristics of alkaline vents would have been; i.e., whether they would have been LCHF-like—resulting from aqueous alteration of olivine-rich crust—or whether they would have been more similar to basalt-hosted vents (Miyazaki and Korenaga 2022; Barnes and Arndt 2019; Papineau et al. 2022) or even vents produced by aqueous alteration of komatiite (Ueda et al. 2021). The Strytan Hydrothermal Field (SHF), Eyjafjord, Iceland, is the only known *alkaline* basalt-hosted hydrothermal vent (Price et al. 2017; Barge and Price 2022, Rucker et al. 2023), and thus represents a crucial analogue for early Earth alkaline hydrothermal systems that could be amenable for origin-of-life processes (Russell and Hall 1997; Russell 2018, 2023). The SHF emits alkaline (pH ~ 10.2), hot (~ 70 °C) freshwater hydrothermal fluids, that are enriched in dissolved SiO_2 and results in precipitation of Mg–silicate (saponite) chimneys up to 55 m tall (Barge and Price 2022; Price et al. 2017; Geptner et al. 2002; Stanulla et al. 2017; Marteinsson et al. 2001). The SHF chimneys host similar pH, redox, and temperature gradients to the LCHF chimneys (Lane & Martin 2012), and in addition, SHF chimneys exhibit a Na^+ gradient between the vent fluid (sourced from meteoric water) and seawater (Price et al. 2017). Previous studies have focused on the microbiology (Marteinsson et al. 2001; Twing et al. 2022) and chimney mineralogy/structure (Stanulla et al. 2017; Geptner et al. 2002) of the SHF; however, the composition of the SHF chimneys has not been characterized in a prebiotic context: i.e., whether the important reactions proposed in a LCHF context would also be likely to occur in a SHF-like early-Earth system.

In the present work we examine material collected from SHF chimneys. We present a structural and compositional overview of two samples of SHF chimneys with scanning electron microscopy (SEM), transmission electron microscopy (TEM), energy-dispersive X-ray spectroscopy (EDX), and X-ray computed tomography (XCT). We compare the vent material with laboratory produced analogue structures from experiments of the type that have been previously used to simulate hydrothermal chimneys (Barge et al. 2019; Hermis et al. 2019). Our goal is to understand whether the SHF chimneys exhibit compositions and mineralogy consistent with reactants and

catalysts necessary to drive prebiotic reactions in an early Earth context.

1.1 The Strytan hydrothermal vent system

An intense hydrothermal activity is observed in many localities in Iceland, due to its location on the Mid-Atlantic Ridge (MAR) and as a mantle hotspot (Celli et al. 2021). Although the common subaerial features are gas emissions, hot springs and mud volcanoes, submarine hydrothermal activity occurs as well. Strytan hydrothermal vents are located in Eyjafjordur, north of Akureyri, 1.8 km offshore in the northeastern part of the fjord. The bedrocks are Tertiary basaltic lavas, 6–12 My old (Bjornsson 1981). Geothermal activity is connected with tectonic features dominating the area, in particular the intersection of NW fault zone and the predominant NNE tectonic trend. However, there are no magmatic inputs, and the only contribution to the hydrothermal system from the MAR is heat. The geothermal field consists of a series of steep cones rising from the seafloor at approximately 70–80 m below sea level. They are aligned along faults, generally trending E–W (Marteinsson et al. 2001). The largest cone reaches approximately 15 m bsl, and is around 55 m in total height. The cones consist predominantly of saponite precipitates, but also contain sediments and shells embedded in the material (Geptner et al. 2002).

The hydrothermal fluids are composed of meteoric rain waters—and are thus fresh—falling on the high ground inland to the south (Marteinsson et al. 2001), that percolate deep into the bedrock and flow tens of km before ascending to the surface through the tectonic features while they draw heat from surrounding rocks. The discharged hydrothermal fluids at Strytan show maximum measured temperature in the active discharge points of approximately 70 °C, high pH values up to 10.2, and high silica content of ~ 94 mg L^{-1} out of a total mineral concentration of 291 mg L^{-1}, (i.e., ~ 1/3 silica) (Marteinsson et al. 2001). Images of the vents where samples were taken for this study are given in Fig. 1A, B.

2 Methods

2.1 Field sample analysis

In August 2017, we performed a field-sampling campaign to the Strytan hydrothermal field (Fig. 1A, B), and scientific scuba divers collected mineral precipitates from two of the cones, Big Strýtan and Arnarnesstrýtan. Precipitates were taken by breaking off small, ~15 cm × 5 cm, pieces and placing them into sterile Whirl–pak bags (Nasco, WI, United States). The samples were stored at four degrees Celsius for transportation and finally dried at room temperature.

Two field samples (S1 and S2) collected from the Strytan vents (Fig. 1C, D) were studied. In sample S1 there were identified two zones, termed S1(tube), owing to the existence of some parallel tubes, and S1(tip) (Fig. 1E). Specific zones of these samples with particular microstructures were investigated: Two zones in sample S2, S2(top), and S2(bottom), were investigated for their different colours (Fig. 1F). These zones were extracted from the whole sample, and portions of these were studied separately. One portion was ground in an agate mortar and analysed by powder X-ray diffraction (XRD). Scanning electron microscopy (SEM) was performed using FEI Quanta 400 and 650 microscopes. Chemical analysis of the micromorphology was determined by EDX analysis. Transmission and analytical electron microscopy (TEM-AEM) was performed in a FEI TITAN G2 microscope, with an XFEG emission gun, a spherical aberration corrector, and a high-angle annular dark-field (HAADF) detector. Samples were ground in an agate mortar, suspended in pure ethanol and dropped on Cu grids. Analyses were performed at 300 kV with a resolution of ~ 0.2 nm in the high-resolution (HRTEM) mode and ~ 2 nm in scanning TEM (STEM) mode (where the STEM method uses an HAADF detector). Compositional analysis was performed with a Super X micro X-ray analyser equipped with four detectors by EDX. In addition, ultrathin sections were prepared with samples encased in resin. X-ray computed tomography (XCT) was performed in an Xradia 510 VERSA tomograph. A 0.4X detector was used. Given that the two samples present a noticeable difference in density, the operating parameters vary from one to another. For S1 we set 80 kV potential, 87 μA current, and a 7 W target power; exposure time was 2 s and pixel size 17.1 μm. For S2, the configuration was set instead to 50 kV potential, 80 μA current, and 3.98 W target power; exposure time was 15 s and pixel size was 12.22 μm. Data processing was performed using Scout and Scan Control System 12.0.8059 and Reconstructor Scout and Scan 12.0.8059. Further data treatment and visualization were carried out with the FIJI distribution of ImageJ including the 3DViewer plugin.

2.2 Laboratory chemical garden experiments

A glass Hell-Shaw cell of 15 mm thickness, 60 mm width and 200 mm height was filled with an aqueous solution of 1 M sodium silicate. An aqueous solution of 1 M magnesium chloride was injected into this reactor by using a motorized syringe at a constant injection rate of 3 mL/hr, following the procedure reported elsewhere (Sainz-Díaz et al. 2018). The experiment was performed in a laboratory maintained at 20 °C. Demineralized and decarbonated water was used in all assays.

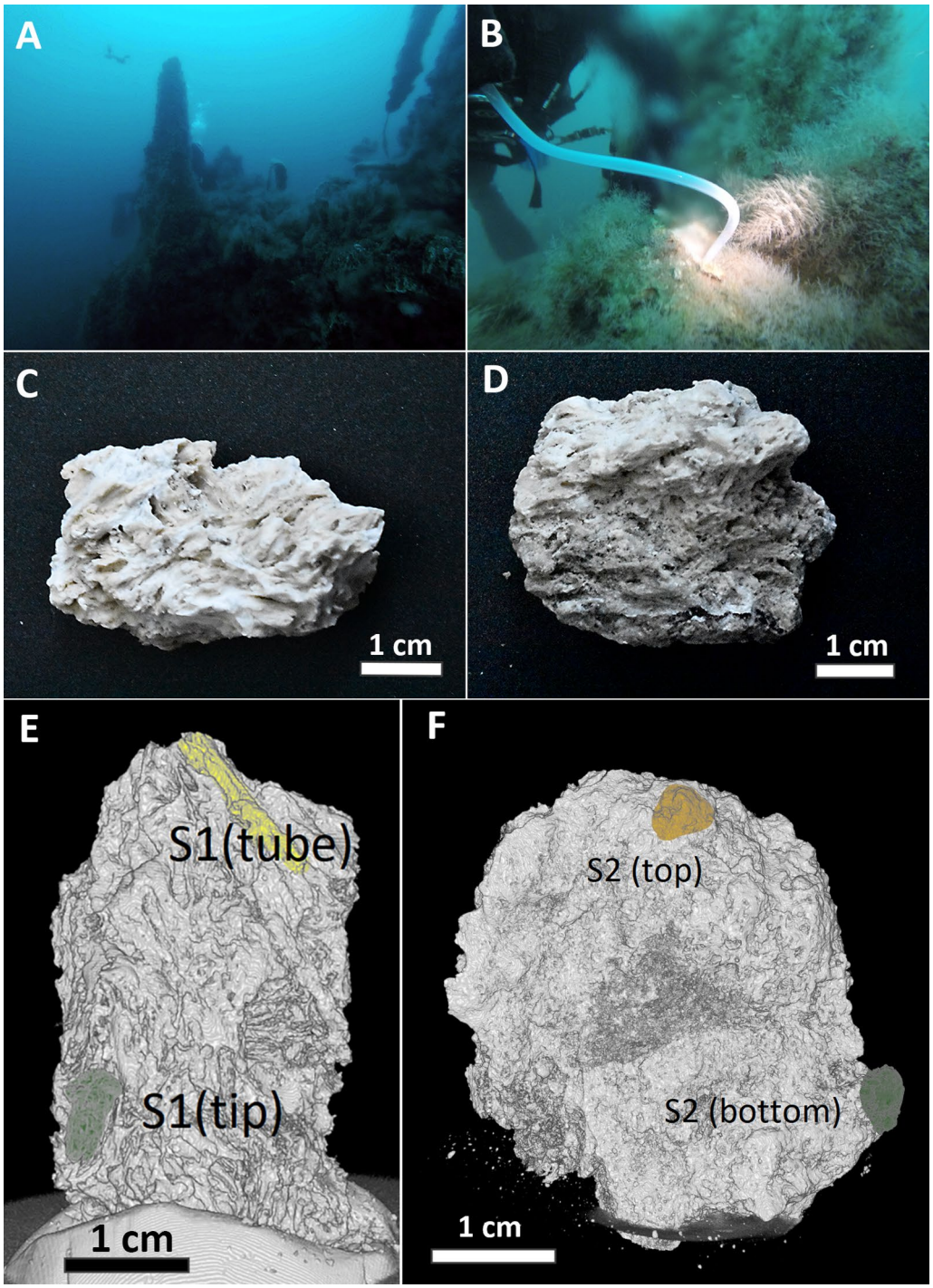

Fig. 1 Chimneys at the Strytan hydrothermal vent system (**A**), Sampling of solids and fluids (**B**). Close up of samples S1 (**C**) and S2 (**D**). Zones identified in samples (**E**) S1; S1(tube) and S1(tip) are in yellow and green, respectively, and (**F**) S2; S2(top) and S2(bottom) are in yellow and green, respectively

For analysing the structures formed in this process, the solid was washed twice with water and dried at air at 45 °C. Micrographs of these solids were obtained by using a FEI-Quanta 400 environmental scanning electron microscope.

3 Results

3.1 Field samples

Sample S1 has a light colour and is highly porous with low density; the sample S2 has a greyish colour and is more compact.

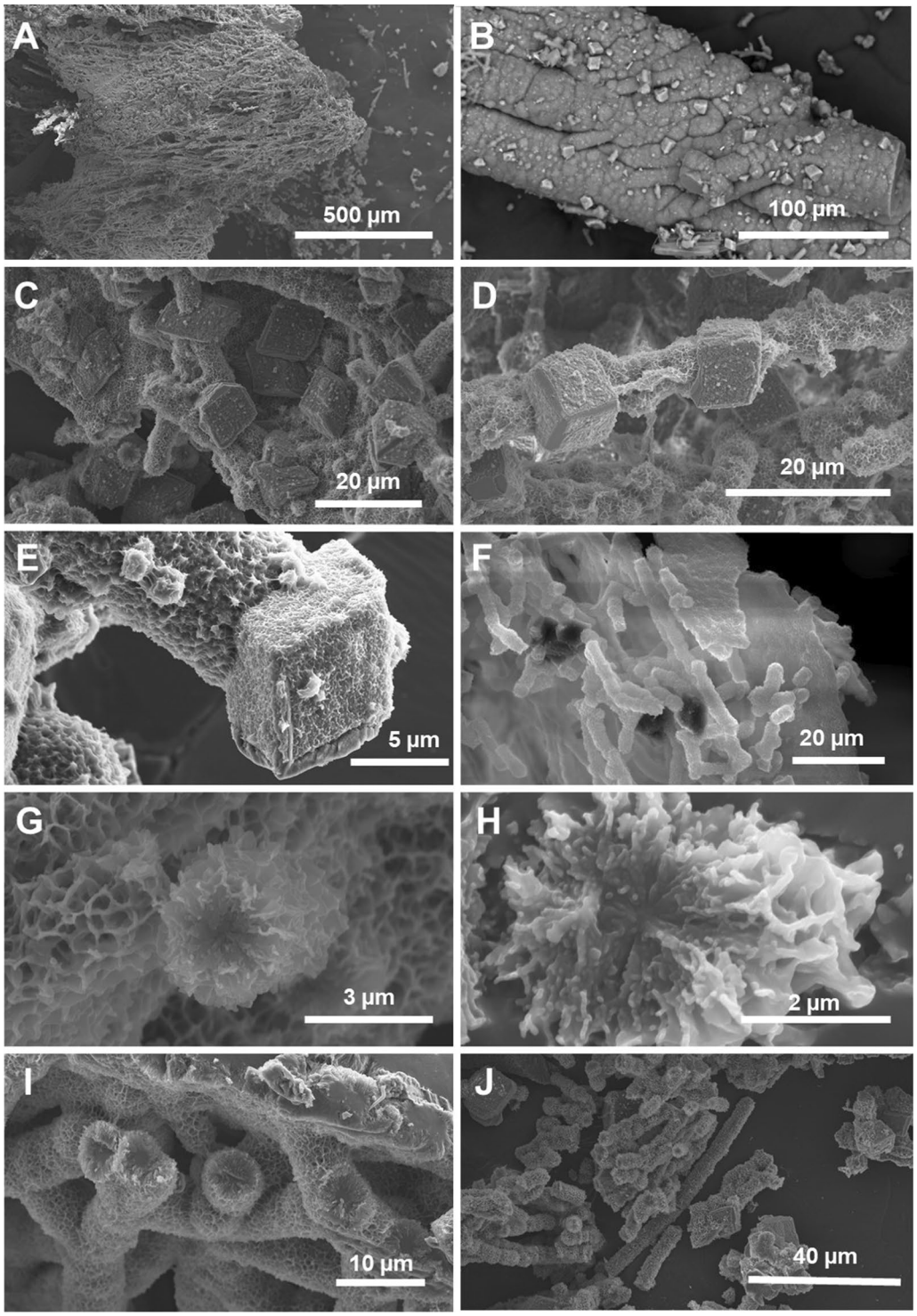

Fig. 2 SEM micrographs of Strytan vent sample S1, light in colour and highly porous

In sample S1 many tubular structures were found growing in disordered groups (Fig. 2A). In many cases isolated rods are observed (Fig. 2B–F). Typical rhombohedral crystals of calcite morphology are found with an average size of 6–10 μm (Fig. 2C–E). This was confirmed with EDX chemical analysis, which showed these crystals are composed of calcium carbonate. They are covered and surrounded by flaky solids that likely precipitated later. The chemical analysis of these flaky solids indicated that they are composed of magnesium silicate. The presence of some rods was detected with an average diameter of 2–5 μm (Fig. 2G–J). The microstructure of these rods shows a compact centre and a flakier structure in the external surface (Fig. 2G-–J). This structural difference indicates two possible growth regimes: one along the rod length and another in a radial direction perpendicular to the central compact rod. We cannot know from this evidence alone, however, whether the regimes are simultaneous or consecutive. These rods can grow in straight forms and in periodic globular chains. At some points along these chains isolated calcite crystals have formed, stopping the chain growth in some cases (Fig. 2E).

In sample S2, the microstructure is different to that of S1. No isolated calcite crystals are observed. Some tubular forms of 5–10 μm in diameter are observed (Fig. 3A–C, H). Some rods similar to those found in sample S1 of a diameter of 2–3 μm (Fig. 3C–D) were found. The microstructure of these rods showed that nanorods of 100 nm diameter grow radially, i.e., normal to the rods' central axes (Fig. 3E). The microstructure of some tubes indicates that globular aggregation units of 100–300 nm form the tubular structure (Fig. 3F, G). Some microspheres of 1 μm are also observed; some of them forming disordered columns (Fig. 3F, G). In some zones compact crystals were observed (Fig. 3I) and other zones are covered by layers of NaCl (Figs. 3J, 4c).

The chemical composition of the samples was determined in situ within the SEM with energy-dispersive X-ray spectroscopy (EDX) analysis of the sample (Fig. 4). In sample S1, carbonate crystals were observed (Fig. 4A left), whose rhombohedral morphology indicates calcite. These crystals are surrounded by a thin layer of a highly porous material presumed to be a magnesium silicate (Fig. 4A, right). In some zones a small amount of Al was also detected in the magnesium silicate solids (Fig. 4B). In sample S2, rods are surrounded by a highly porous material identified as magnesium silicate. In some cases, the relative Mg/Si proportion increases along with the oxygen content in the external border of this material (Fig. 4D left). These changes in the chemical content can be assigned to the formation of magnesium hydroxide along with silicate layers. In the external zones of magnesium silicate materials with a higher Al content has been observed (Fig. 4D, bright zones in the left zones), whereas the internal zones the amount of Al is negligible (Fig. 4D, bright zones in the right side). Since the vent fluid is the source of aqueous Al^{3+}, this change in precipitate composition from inner to outer would indicate a change in the precipitation conditions (Fig. 4D). Some phases with low porosity are identified as calcium carbonate and sodium chloride (Fig. 4C). Some rods are generated from nuclei of calcium sulfate (Fig. 4F).

XRD data show that the S1(tip) sample has crystals of aragonite and calcite (Fig. 5A) along with saponites of low crystallinity showing broad peaks. The S1(tube) sample shows calcite crystals and saponite (Fig. 5B). The S2(top) sample shows crystals of saponite and calcite (Fig. 5C). Finally, sample S2(bottom) shows a similar composition, but with more saponite (Fig. 5D).

The overall TEM pictures show some dense particles surrounded by a disordered fringing material (Fig. 6A). HRTEM micrographs showed layered morphology in many particles of all samples. This material consists of smectite-like particles grown from the alteration of magnesium silicate precipitated from the alkaline waters, as observed above in Fig. 6D. The layered particles correspond to aggregates of flakes, a few hundred nm or less in size. They consist of aggregates of curved or folded lamellar particles (Fig. 6B). The crystallinity of these materials is very low, and no small-angle electron diffraction (SAED) patterns could be obtained. In some cases, spacings of 10 to 16 Å can be identified, with scarce lateral continuity and numerous stacking defects. These spacings and the texture of the aggregates indicate that they are probably smectite lamellae (Fig. 6C). The dark particles correspond to denser grains, with no apparent internal structure, since in no case have lattice fringes or diffraction patterns been observed. Probably these particles correspond to fragments of larger particles, which have been disaggregated during the sample preparation procedure. They often present a reticulated and spongy rim, in which curved and folded lamellae are seen, similar to those observed in flaky particles. In some cases, they also present lattice fringes corresponding to basal spacings of smectite-like minerals. The images obtained in ultrathin sections showed that the dense particles without crystalline structure correspond to the interior of large particles, which are externally surrounded by a rim of smectite lamellae. This morphological evolution suggests that the smectites were formed by a process of alteration and precipitation involving previously formed amorphous magnesium silicates. Spherical particles consisting of a core surrounded by lamellae, similar to those observed in larger particles, were also observed (Fig. 6D).

Chemical analyses of individual particles or small areas were obtained in STEM mode (Additional file 1:

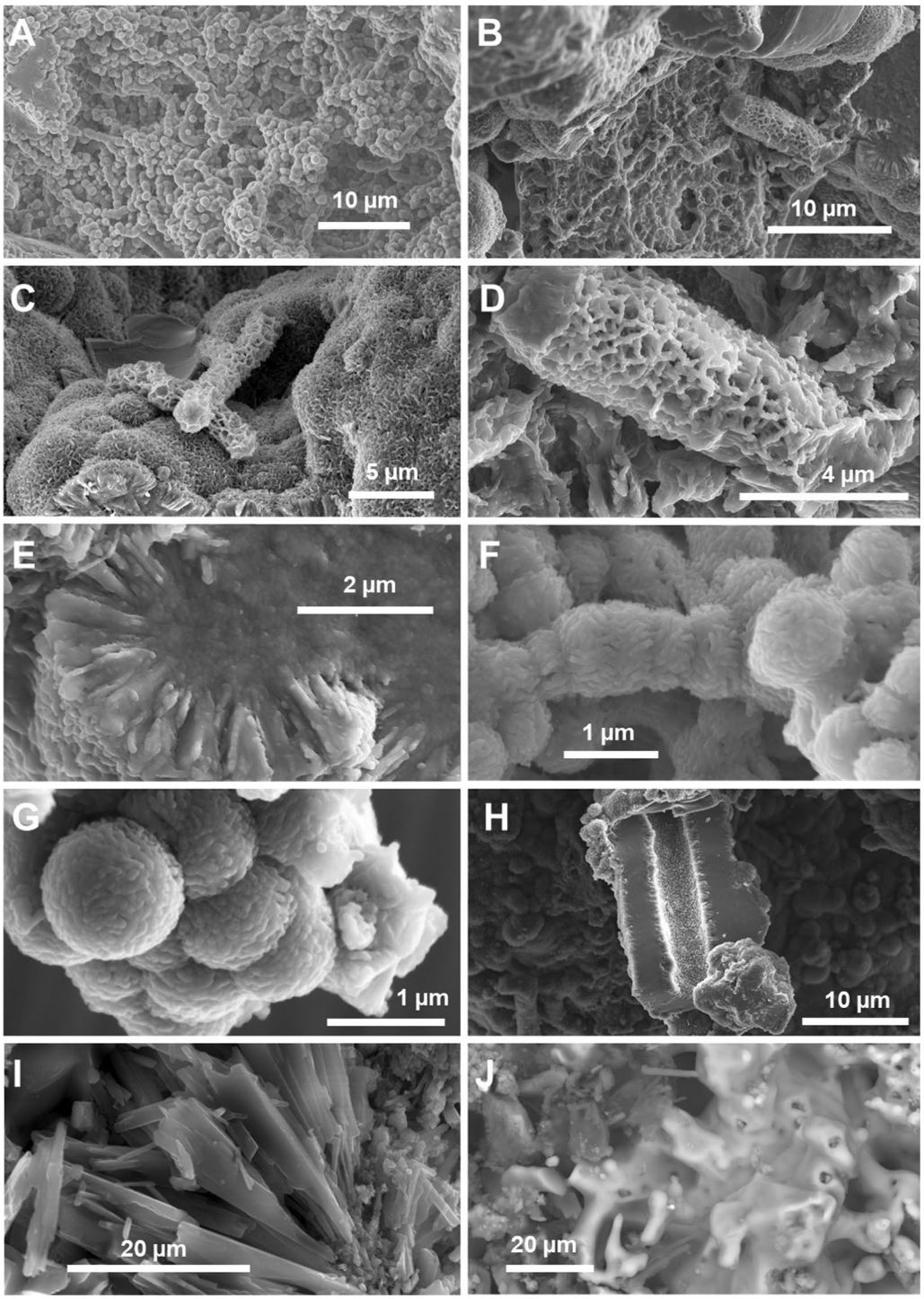

Fig. 3 SEM micrographs of Strytan vent sample S2, grey in colour and compact

Table S1). Intensity ratios were recalculated as oxide composition. The samples are mostly composed of Mg and silica, with variable Al content, as well as minor amounts of Fe, alkali and alkaline earth cations. Plotting the analyses on a SiO_2-($Al_2O_3 + Fe_2O_3$)-MgO ternary plot (Fig. 7), the dots are seen to be located next to the SiO_2-MgO line, with $Al_2O_3 + Fe_2O_3 < 10\%$. Analyses of flaky structures are compatible with Mg phyllosilicates

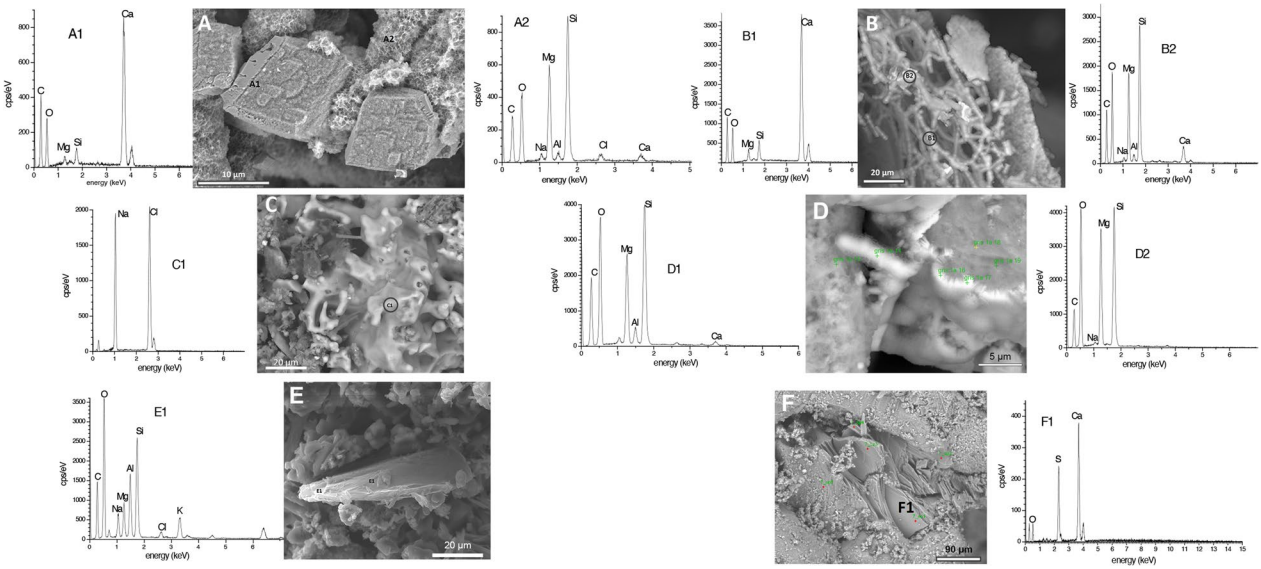

Fig. 4 EDX analysis of SEM images of field samples. **a**–**b** S1, **c**–**f** S2

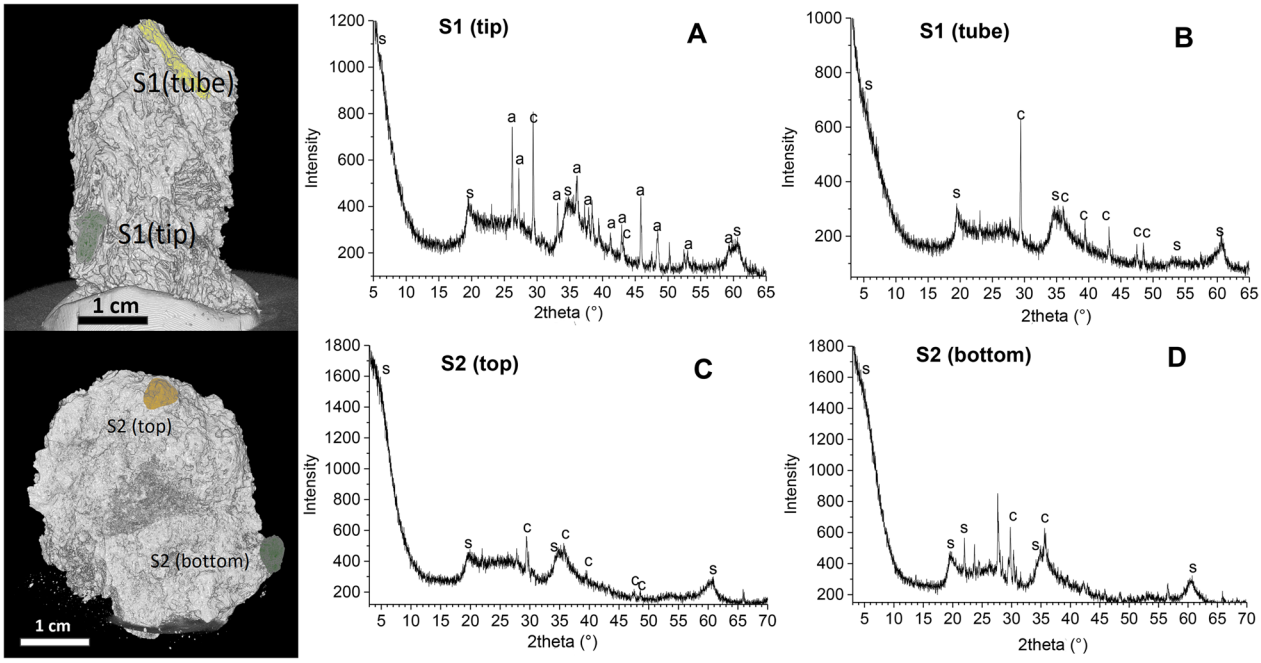

Fig. 5 Powder X-ray diffraction patterns of the sample S1(tip) (**A**), S1(tube) (**B**), S2(top) (**C**), and S2(bottom) (**D**). Most of the reflections may be assigned to aragonite (**a**), calcite (**c**), and saponite (s)

of the saponite-stevensite type (Fig. 7, dark colour). The calculation of the structural formulae was carried out on non-homoionic (raw) samples, so that a part of the Mg content should be located in the interlayer space as an exchangeable cation. Structural formulas were estimated on the basis of $O_{10}(OH)_2$, that correspond to half unit cell for a smectite. Si and Al were assigned to the tetrahedral layer up to 4 cations; the remaining Al together with Fe and Mg were assigned to the octahedral layer up to 3. Fe was estimated as Fe(III). Mg was divided between octahedral and interlayer positions using charge balance as a criterion. The composition of these particles is within a limited area that corresponds to the saponite-stevensite smectites.

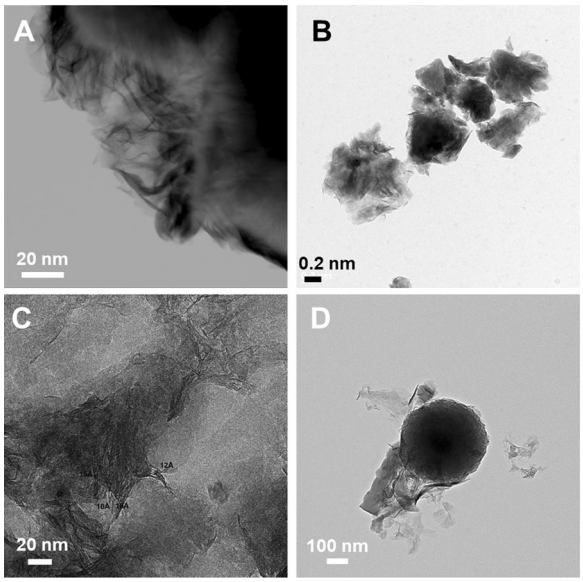

Fig. 6 HRTEM micrographs of samples S1 (**a**–**c**) and S2 (**d**)

The analyses of those particles that show neither crystal arrangements nor layered morphology (Fig. 7, light colour) are divided into three groups. The first one includes most of the analyses of S2(bottom) and some S2(top) particles, which are grouped in a narrow range of compositions (approximately SiO_2 60–63%, MgO 35–37%, $Al_2O_3 + Fe_2O_3 < 1\%$), close to the Mg-richer saponites. Most of the S1(tube) particles belong to the second group and correspond to compositions richer in silica than saponites and extended over a wide range of compositions (SiO_2 65–80%, MgO 15–27, $Al_2O_3 + Fe_2O_3$ 1.5–5.5%). In contrast, the third group comprises the analysis of a few S2(top) particles. These particles are very rich in silica (72–76%), but the content of trivalent cations (13–16%) is much higher than that of MgO (3–8%).

These results indicate that the particles are composed of magnesium silicate, with an important variability of the ratio between both elements, which reflects a certain heterogeneity of the material. Other cations are in the minority, except for the third group already mentioned.

The heterogeneity of the composition of the clays in the chimney can be seen in Fig. 8. This corresponds to a fragment with a dense core surrounded by lamellar structures, as well as another deposit of small rounded particles, smaller than 100 nm. All analyses have been recalculated as smectite structural formulas for comparison (Additional file 1: Table S1). The chemical analysis #4 of the core is compatible with a Mg smectite, although its lack of internal structure and its morphology do not correspond to a smectite. Analyses #2 and #5 correspond to laminated textures and can be identified as saponite. The slight positive octahedral charge may be due to part of the Mg occupying interlaminar positions. The analysis of the laminations in area #6 would be compatible with a very low charge stevensite, and a fraction of the Mg could also occupy interlaminar positions. On the other

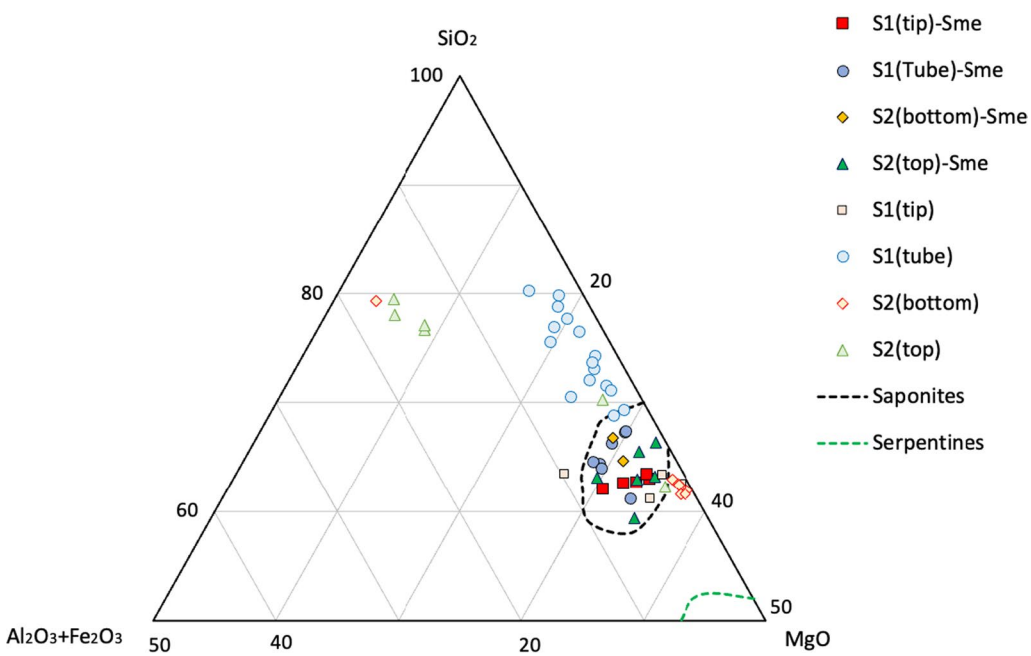

Fig. 7 Ternary diagram and composition of the clay minerals found in the Strytan vent samples. Dark colour, layered particles; light colour, other morphologies

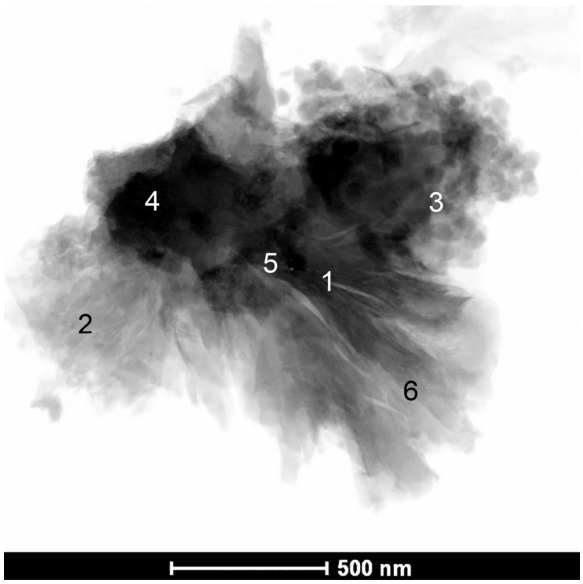

Fig. 8 HAADF analysis of chimney composition. Numbers correspond to values in Table 1

hand, the analysis of area #1, with a laminar texture similar to #5 or #6, presents an excess of Mg that leads the calculated formula to have a deficit of Si and Al. Finally, the analysis of the rounded particles of area #3 shows an excess of Si and a very high Al content, allowing a probable identification as a smectite.

The results of the punctual analysis show compositional heterogeneity in the particles. The general composition is magnesium silicate, with local predominance of Si or Mg, and presence of other cations. The lamellar structures, which can be assimilated to smectites, have low crystallinity and numerous lattice defects. In addition, between the lamellae there are remains of the original amorphous material or of cations leached during the alteration and formation of smectites. This may be the cause of smectite particles whose structural formula has an excess or defect of cations.

With X-ray computed tomography, Fig. 9, we note how the greyish sample S2 has a more compact structure with fewer and smaller pores showing thicker walls and a more robust construction than S1.

3.2 Laboratory chemical gardens

Similar flaky morphology is observed in chemical garden materials formed in the laboratory with magnesium chloride solution injected into sodium silicate solution, being mainly magnesium silicate with a high proportion of magnesium hydroxide (Fig. 10) (Sainz-Díaz et al. 2018).

4 Discussion

4.1 SHF chimneys compared to other vent types

Our investigations of the SHF field samples are consistent with previous literature regarding the presence of smectite/saponite clays, amorphous silica, gypsum, and carbonates (Geptner et al. 2002; Price et al. 2017; Marteinsson et al. 2001; Stanulla et al. 2017). We additionally report the presence of magnesium hydroxide in the SHF field samples. This has been reported at other alkaline vents, including LCHF and Prony Hydrothermal Field (Proskurowski et al. 2008; Pisapia et al. 2017; and also see Okumura et al. 2016a, b), but has not been previously detected in SHF chimneys (Price et al. 2017; Russell 2017). Though magnesium hydroxide may be difficult to detect in these field samples, it makes sense that it should form in this system, as it is seen in chemical-garden experiments of precipitation of Mg salts into silicate solutions, where both Mg–silicate and Mg oxide/hydroxide are abundant in the resulting precipitates (Sainz-Diaz et al. 2018; and Fig. 10).

The SHF chimneys also bear similarities to LCHF that are relevant in an early-Earth context. The SHF chimneys have a microporous, labyrinthine interior structure (Fig. 9) that is similar to observed interior structures of other alkaline vents such as LCHF (Kelley et al. 2005) or Prony (Jones et al. 2020); and is different than chimneys

Table 1 Chemical composition of points in particle in Fig. 8

Cation	1	2	3	4	5	6
Si	3.80	3.85	4.37	3.76	3.82	3.96
Al	0.16	0.16	0.96	0.49	0.28	0.18
Mg	3.11	2.99	0.38	2.53	2.87	2.76
Fe(III)	0.00	0.01	0.02	0.00	0.00	0.00
Na	0.00	0.00	0.49	0.14	0.00	0.00
K	0.00	0.01	0.19	0.03	0.00	0.01
Ca	0.05	0.04	0.06	0.13	0.06	0.04

Chemical analysis was converted to cations on the basis of $O_{10}(OH)_2$. Analyses 2, 4, and 5 are compatible with Mg smectites

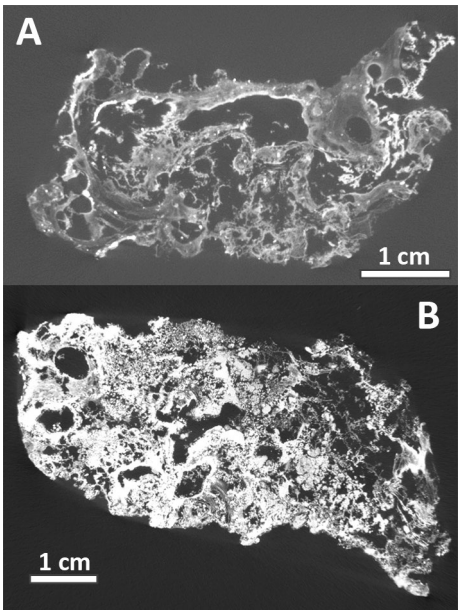

Fig. 9 µCT slices showing the inner structures of S1 (top) and S2 (bottom) samples

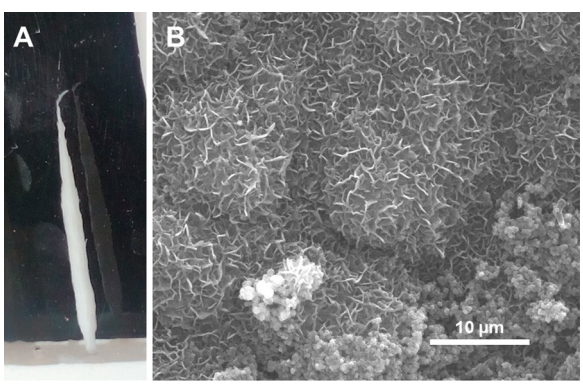

Fig. 10 A chemical garden formed in laboratory experiments from 1 M Mg chloride and 1 M silicate solution (**a**) and an SEM image (**b**) of the internal surface of the material formed

of black or white smokers, which exhibit denser, more cemented interiors with defined fluid flow conduits (Tivey and Singh 1997). This similarity between alkaline vents is likely due to the slower, diffuse flows that occur in alkaline vent chimneys compared to the hotter, faster flows that occur in the smoker vent chimneys (Von Damm 1990).

In an origin-of-life context both the lifetime of the Vent (i.e., the timeline for which the hydrothermal flow remains active) and the rate of chimney growth (since this determines its structure) are important. We can use fluid mechanics to model the growth rate of the chimney precipitate over time. The Strytan hydrothermal vent is a geological chemical garden, similar to Sainz-Diaz et al. (2018) but with interior and exterior solutions reversed and different chemistry, where, driven by osmosis, high Si enriched vent fluid reacts and precipitates with cations in the surrounding seawater. For slow osmosis, the wall thickness of a chemical garden L_m over time is given by (Ding et al 2019):

$$L_{\mathrm{m}}^2 = \frac{2\underline{M}k_{\mathrm{in}}p_{\mathrm{o}}c_{\mathrm{Si}}}{\mu\rho_{\mathrm{S}}}t$$

here c_{Si} is the concentration of the external silicate solution, p_{o} is the osmotic pressure, k_{in} is the permeability of the membrane in the regions of inflow, μ is the viscosity of the fluids, ρ_{s} is the precipitate density. For the Strytan hydrothermal vent precipitates, calculating from data in the literature, the permeability is 0.4×10^{-15} to 10^{-14} m^2 (Price et al. 2017; Geptner et al. 2002), thus, taking a value in the middle of that range, allowing for calculation of the chimney wall growth rate. The osmotic pressure is calculated with consideration of all the ions of sea water and vent water; the osmotic coefficient for the sea water $\phi = 0.907$, the vent water is dilute and $\phi = 1.0$. We estimate the density of the rock, ~ 3 kg/L, as 10 times higher than the overall density of porous samples, 0.3–0.5 kg/L. We may compare this calculation with the growth of black smoker and LCHF vent chimneys (Cardoso and Cartwright 2017), as shown in Fig. 11. We find that Strytan will have faster growth compared with chemical diffusion of Lost City, but is still much slower compared to a black smoker, which grows by thermal diffusion. The predicted growth rate of Strytan is compatible with a hypothesis that the cones could have started growing at the end of the last glacial maximum, ~ 18 k y ago; compare with the > 30,000 years predicted for the LCHF (Früh-Green et al. 2005).

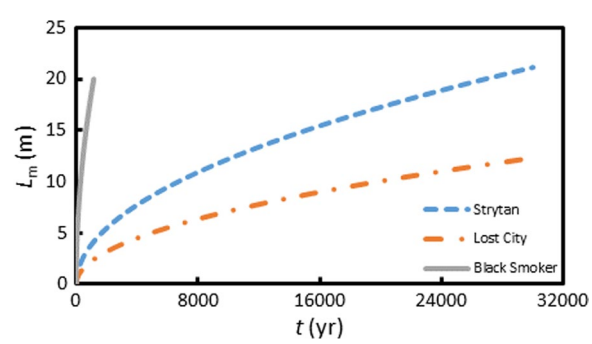

Fig. 11 Fluid-mechanical prediction of the growth of a Strytan vent over time in terms of wall thickness L_m (blue) compared with black smokers (grey) and LCHF (orange) vents

4.2 SHF-like vents in an early Earth context

An important issue for prebiotic early-Earth alkaline vents is what types and chemistries of vents and chimneys were likely to be present, given different host rock and ocean composition. The basaltic host rock of the Strytan vents is similar to typical mid-ocean ridge basalts, MORB (Arnórsson et al. 2002; Price et al. 2017). In contrast, the LCHF is produced by olivine-rich mantle rock that is exposed to seawater during seafloor spreading at the mid-Atlantic ridge, yielding its alkaline fluids, brucite/carbonate chimneys, and high concentrations of H_2 and CH_4 (Kelley et al. 2001, 2005; Früh-Green et al. 2003). However, it is debated when plate tectonics began and if it was operating on early Earth around the time of the origin of life; this is important since it determines the rock composition of the ocean crust that would form hydrothermal vents. On one hand, it has been argued that Earth had an early onset of plate tectonics that resulted in olivine-rich ocean crust that would facilitate serpentinization, and thus, LCHF-like vents (Miyazaki and Korenaga 2022; Debaille et al. 2013; Deng et al. 2023); alternatively, it has been argued that Hadean Earth was in a stagnant-lid regime without geochemical cycling from plate tectonics (Tarduno et al 2023). Komatiites, MgO-rich igneous rocks that appear almost exclusively in the Archean rock record, and form at hotter mantle temperatures (Barnes and Arndt 2019; Takahashi and Scarfe 1985; Grosch and Wilson 2023), may have been a predominant seafloor crust rock on the early Earth, along with other Archean basalts, which could have been in some ways similar to modern MORB (Barnes and Arndt 2019; O'Neil et al. 2012). There has been limited experimental work on aqueous alteration of komatiite, but a recent study has shown that H_2 concentrations, as well as pH in komatiite-produced "hydrothermal fluids" increased at higher temperatures (~300 °C) (Ueda et al. 2021), meaning that on early Earth, hotter vents with black-smoker temperatures might have had pH and redox gradients similar to Strytan or LCHF. Another consequence of early Earth's hotter mantle is potential seafloor shallowing leading to volcanic islands creating exposed land mass (Rosas and Korenaga 2021); Archean basalt-hosted shallow vents could have also existed on the coasts of volcanic islands (Barge and Price 2022).

The interface of alkaline hydrothermal fluid, rich in OH^-, Mg^{2+}, and HS^- (Mielke et al. 2010; White et al. 2020), with the early Earth's ocean, anoxic, rich in dissolved Fe^{2+}, SiO_2, and CO_2 (MacLeod et al. 1994; Halevy and Bachan 2017; Tosca et al. 2016) would have resulted in chimney precipitates containing minerals similar to those at Strytan (Mg-silicates and clays, calcium carbonates, magnesium hydroxides), but also Fe-hydroxides, Fe-carbonates, greenalite and/or silica gels, and perhaps Fe–Mg-containing clays (Ferris et al. 1986, Ferris 2005, 2006 Meunier et al. 2010, Russell 2018, 2017; Barge et al. 2020; Tosca et al. 2016; Halevy et al. 2017). If the early-Earth vents were, like Strytan, in shallow waters (e.g., Barge and Price 2022), then the chimney mineralogy could also have been influenced by photochemically produced species. For example, NO_3^-/NO_2^- could have acted as oxidants to produce Fe^{3+} from Fe^{2+} (Wong et al. 2017; Ranjan et al. 2019); or Fe^{2+} could also have been oxidized directly by UV radiation (Nie et al. 2017). This would have resulted in precipitation not just of Fe(II)-minerals, but also mixed-valence Fe(II,III) minerals, including green rust (Russell 2018; Halevy et al. 2017). Green rust, fougerite, has been proposed to be important for driving a variety of prebiotic reactions toward the emergence of metabolism (Russell et al. 2018, 2023; Branscomb and Russell 2013).

The metastable Fe-containing analogue of brucite (ferrobrucite) forms in serpentinizing systems even today (Templeton and Ellison 2020) and is theorized to have existed at LCHF-like vents on the early Earth (Trolard et al. 2022). Our detection of magnesium hydroxide along with silicates in the Strytan chimneys is significant since it implies that, in the early Fe^{2+}-bearing oceans, Strytan-like chimneys would also contain iron-bearing minerals such as ferrobrucite or green rust, and could thus support LCHF-like prebiotic chemistry. Potential early-Earth LCHF-like prebiotic reactions driven by Fe-hydroxide and Fe-sulfide minerals: e.g., carbon reduction, amino acid synthesis, peptide formation, phosphorous chemistry, have been discussed at length in the literature (e.g., Russell 2023, 2018; White et al. 2015; Roldan et al. 2015; Barge et al. 2019, 2020, Hudson et al 2020). However, in contrast to a LCHF-like chimney, a Strytan-like chimney would additionally host reactions driven by silicate minerals such as Fe/Mg-clays (saponite), greenalite, and silica gels. This could include aromatic amino acid synthesis by Fe/Mg-saponites (e.g., Ménez et al. 2018); dehydration and/or condensation reactions in silica gels (e.g. Westall et al. 2018; Gorrell et al. 2017; Dass et al. 2018); or polymerization of RNA-type molecules catalysed by greenalite particles (e.g. Rasmussen et al. 2021).

5 Conclusions

The Strytan field samples investigated in this work have properties of interest to prebiotic chemistry in a Strytan-like system on the early Earth. Similar to the pore structure of other alkaline vent chimneys, the Mg–silicate chimneys are porous and contain a labyrinthine internal structure. Chemical analysis of the chimneys is consistent with previous studies, demonstrating the presence of clays and silicate minerals, but in this study we also

detected Mg-hydroxide. This implies that Strytan-like vents on early Earth could have hosted LCHF-like prebiotic chemistries driven by iron-containing magnesium hydroxide and/or perhaps other Fe-hydroxides. Thus Strytan may be an even higher-fidelity early-Earth analogue than the LCHF, because of its basalt host rock. Further studies of the SHF and other basalt-hosted vents, as well as further laboratory experiments simulating the growth of hydrothermal chimneys, can continue to shed light on the prebiotic reactions that could have been favoured in these kinds of systems.

Supplementary Information

The online version contains supplementary material available at https://doi.org/10.1186/s40645-023-00603-w.

Additional file 1. Table S1. Chemical composition (in oxides wt%) of particles analysed by TEM-EDS.

Acknowledgements
This research was supported in part by the ELSI Origins Network (EON), which was supported by a grant from the John Templeton Foundation. REP acknowledges NASA Habitable Worlds Program Grant Nos. 80NSSC20K0228 and 80NSSC24K0076. SEM acknowledges JSPS KAKENHI Grant No. 22K18278. LMB's work was performed at the Jet Propulsion Laboratory, California Institute of Technology under a contract with NASA (80NM0018D004). This research was funded in part by Spanish FEDER/Junta de Andalucía-Consejería de Economía y Conocimiento grant PY20_01389. We acknowledge the contribution of the COST Actions CA17120, Chemobrionics and CA21169, Dynalife, supported by European Cooperation in Science and Technology.

Author contributions
Conception and design: SEM, CISD, JHEC; Sample collection: SEM, DG, RP; Data analysis, curation, methodology: CGA, LMB, YD, SSSC, SEM, RN, DG, RP, FJH, CISD, JHEC; Visualization: CGA, YD; Wrote the initial manuscript draft: LMB, CISD, JHEC; Organized the expedition and acquired funding: SEM; Interpretation, review, editing: LMB, SSSC, SEM, DG, RP, FJH, CISD, JHEC.

Funding
Open Access funding provided thanks to the CRUE-CSIC agreement with Springer Nature. This research was supported in part by the ELSI Origins Network (EON), which was supported by a grant from the John Templeton Foundation. REP acknowledges NASA Habitable Worlds Program Grant Nos. 80NSSC20K0228 and 80NSSC24K0076. SEM acknowledges JSPS KAKENHI Grant No. 22K18278. LMB's work was performed at the Jet Propulsion Laboratory, California Institute of Technology under a contract with NASA (80NM0018D004). This research was funded in part by Spanish FEDER/Junta de Andalucía-Consejerí de Economí y Conocimiento grant PY20_01389. We acknowledge the contribution of the COST Actions CA17120, Chemobrionics and CA21169, Dynalife, supported by European Cooperation in Science and Technology.

Availability of data and materials
The materials used and/or analysed during the current study are available from the corresponding author on reasonable request.

Declarations

Competing interests
We have no competing interests.

Received: 20 September 2023 Accepted: 21 December 2023
Published online: 29 February 2024

References

Alan F, Desbruyères D, Kim Juniper S (1987) Deep-sea hydrothermal vent communities at 13°N on the east Pacific RISE: microdistribution and temporal variations. Biol Oceanogr 4(2):121–164
Arnórsson S, Gunnarsson I, Stefansson A, Andrésdóttir A, Sveinbjörnsdóttir A (2002) Major element chemistry of surface- and ground waters in basaltic terrain, N-Iceland: I. Primary mineral saturation. Geochim Cosmochim Acta 66:4015–4046
Barge LM, Flores E, Baum MM, VanderVelde D, Russell MJ (2019) Redox and pH gradients drive amino acid synthesis in iron oxyhydroxide mineral systems. Proc Natl Acad Sci 116(11):4828–4833
Barge LM, Price RE (2022) Diverse geochemical conditions for prebiotic chemistry in shallow-sea alkaline hydrothermal vents. Nat Geosci 15:976–981
Barge LM, Jones JP, Pagano JJ, Martinez E, Bescup J (2020) Three-dimensional analysis of a simulated prebiotic hydrothermal chimney. ACS Earth Space Chem 4:1663–1669
Barnes SJ, Arndt NT (2019) Earth's oldest rocks, 2nd edn. Elsevier, Amsterdam, pp 103–132
Barthélémy K et al (2012) Carbonated ferric green rust as a new material for efficient phosphate removal. J Colloid Interface Sci 384(1):121–127
Bjornsson A (1981) Exploration and exploitation of low-temperature geothermal fields for district heating in Akureyri, North Iceland. Geotherm Resour Counc Trans 5:495–498
Branscomb E, Russell MJ (2013) Turnstiles and bifurcators: the disequilibrium converting engines that put metabolism on the road. Biochim Biophys Acta BBA Bioenerg 1827(2):62–78
Cardoso SSS, Cartwright JHE (2017) On the differing growth mechanisms of black-smoker and Lost City-type hydrothermal vents. Proc R Soc A 473(2205):20170387
Celli NL, Lebedev S, Schaeffer AJ, Gaina C (2021) The tilted Iceland Plume and its effect on the North Atlantic evolution and magmatism. Earth Planet Sci Lett 569:117048
Dass AV, Jaber M, Brack A, Foucher F, Kee TP, Georgelin T et al (2018) Potential role of inorganic confined environments in prebiotic phosphorylation. Life 8:7
Debaille V, O'Neill C, Brandon AD, Haenecour P, Yin QZ, Mattielli N, Treiman AH (2013) Stagnant-lid tectonics in early Earth revealed by 142Nd variations in late Archean rocks. Earth Planet Sci Lett 373:83–92
Deng Z, Schiller M, Jackson MG, Millet MA, Pan L, Nikolajsen K, Saji NS, Huang D, Bizzarro M (2023) Earth's evolving geodynamic regime recorded by titanium isotopes. Nature 621:100–104
Ding Y, Gutiérrez-Ariza CM, Ignacio Sainz-Díaz C, Cartwright JHE, Cardoso SSS (2019) Exploding chemical gardens: A phase-change clock reaction. Angew Chem 131(19):6273–6279
Etique M et al (2014) Nitrate reduction by mixed iron(II-III) hydroxycarbonate green rust in the presence of phosphate anions: The key parameters influencing the ammonium selectivity. Water Res 62:29–39
Ferris JP (2005) Mineral catalysis and prebiotic synthesis: montmorillonite-catalyzed formation of RNA. Elements 1:145–149
Ferris JP (2006) Montmorillonite-catalysed formation of RNA oligomers: the possible role of catalysis in the origin of life. Phil Trans R Soc B 361:1777–1786
Ferris JP, Huang CH, Hagan WJ Jr (1986) Clays as prototypical enzymes for prebiological formation of phosphate esters. Orig Life Evol Biosph 17:173–174
Früh-Green GL et al (2003) 30,000 years of hydrothermal activity at the lost city vent field. Science 301(5632):495–498
Gamo T, Masuda H, Yamanaka T et al (2004) Discovery of a new hydrothermal venting site in the southernmost Mariana Arc: al-rich hydrothermal plumes and white smoker activity associated with biogenic methane. Geochem J 38:527–534
Geptner A, Kristmannsdóttir H, Kristjansson J et al (2002) Biogenic saponite from an active submarine hot spring, Iceland. Clays Clay Miner 50:174–185
Gorrell IB, Henderson TW, Albdeery K, Savage PM, Kee TP (2017) Chemical transformations in proto-cytoplasmic media phosphorus coupling in the silica hydrogel phase. Life 7:45

Grosch EG, Wilson A (2023) The discovery and petrogenetic significance of komatiites. J Afrcan Earth Sci 205:105002
Halevy I, Bachan A (2017) The geologic history of seawater pH. Science 355:1069–1071
Halevy I, Alesker M, Schuster EM, Popovitz-Biro R, Feldman Y (2017) A key role for green rust in the Precambrian oceans and the genesis of iron formations. Nat Geosci 10:135–139
Hansen HCB, Gulberg S, Erbs M, Koch CB (2001) Kinetics of nitrate reduction by green rusts: effects of interlayer anion and Fe(II): Fe(III) ratio. Appl Clay Sci 18:81–91
Hermis N, Barge LM, Melwani Daswani M (2019) Simulation of magnesium silicate hydrothermal chimney system. American geophysical union, fall meeting 2019, abstract #P53D-3488
Hudson R, de Graaf R, Strandoo Rodin M, Ohno A, Lane N, McGlynn SE, Yamada YM, Nakamura R, Barge LM, Braun D, Sojo V (2020) CO_2 reduction driven by a pH gradient. Proc Natl Acad Sci 117(37):22873–22879
Jiang CZ, Tosca NJ (2019) Fe(II)-carbonate precipitation kinetics and the chemistry of anoxic ferruginous seawater. Earth Planet Sci Lett 506(2019):231–242
Jones J-P, Firdosy SA, Barge LM, Bescup JC, Perl SM, Zhang X, Pate AM, Price RE (2020) 3D printed minerals as astrobiology analogs of hydrothermal vent chimneys. Astrobiology 20(12):1405–1412
Kelley DS, Karson JA, Blackman DK, Früh-Green GL, Butterfield DA, Lilley MD, Olson EJ, Schrenk MO, Roe KK, Lebon GT, Rivizzigno P, The AT3-60 Shipboard Party (2001) An off-axis hydrothermal vent field near the Mid-Atlantic Ridge at 30N. Nature 412:145–149
Kelley DS, Karson JA, Früh-Green GL, Yoerger DR, Shank TM, Butterfield DA, Hayes JM, Schrenk MO, Olson EJ, Proskurowski G, Jakuba M, Bradley A, Larson B, Ludwig K, Glickson D, Buckman K, Bradley AS, Brazelton WJ, Roe K, Bernasconi SM, Elend MJ, Lilley MD, Baross JA, Summons RE, Sylva SP (2005) A serpentinite-hosted ecosystem: the lost city hydrothermal field. Science 307:1428–1434
Kormas KA, Tivey MK, Von Damm K, Teske A (2006) Bacterial and archaeal phylotypes associated with distinct mineralogical layers of a white smoker spire from a deep-sea hydrothermal vent site (9°N, East Pacific Rise). Environ Microbiol 8(5):909–920
Lane N, Martin WF (2012) The origin of membrane bioenergetics. Cell 151:1406–1416
Lecoeuvre A, Ménez B, Cannat M et al (2021) Microbial ecology of the newly discovered serpentinite-hosted Old City hydrothermal field (southwest Indian ridge). ISME J 15:818–832
Ludwig KA, Kelley DS, Butterfield DA, Nelson BK, Früh-Green G (2006) Formation and evolution of carbonate chimneys at the Lost City hydrothermal field. Geochim Cosmochim Acta 70:3625–3645
Macleod G, McKeown C, Hall AJ, Russell MJ (1994) Hydrothermal and oceanic pH conditions of possible relevance to the origin of life. Orig Life Evol Biosph 24:19–41
Marteinsson VT, Kristjánsson JK, Kristmannsdóttir H, Dahlkvist M, Sæmundsson K, Hanningtion M, Pétursdóttir SK, Geptner A, Stoffers P (2001) Discovery and description of giant submarine smectite cones on the seafloor in Eyjafjordur, northern Iceland, and a novel thermal microbial habitat. Appl Environ Microbiol 67:827–833
Martin W, Baross J, Kelley D, Russell MJ (2008) Hydrothermal vents and the origin of life. Nat Rev Microbiol 6:806–814
Ménez B, Pisapia C, Andreani M et al (2018) Abiotic synthesis of amino acids in the recesses of the oceanic lithosphere. Nature 564:59–63
Meunier A, Petit S, Cockell CS, El Albani A, Beaufort D (2010) The Fe-rich clay microsystems in basalt-komatiite lavas: importance of Fe-smectites for pre-biotic molecule catalysis during the Hadean eon. Origins Life Evol Biosph 40(3):253–272
Mielke RE, Russell MJ, Wilson PR, McGlynn SE, Coleman M, Kidd R, Kanik I (2010) Design, fabrication, and test of a hydrothermal reactor for origin-of-life experiments. Astrobiology 10(8):799–810
Miyazaki Y, Korenaga J (2022) A wet heterogeneous mantle creates a habitable world in the Hadean. Nature 603:86–90
Monnin C, Chavagnac V, Boulart C, Ménez B, Gérard M, Gérard E et al (2014) Fluid chemistry of the low temperature hyperalkaline hydrothermal system of Prony Bay (New Caledonia). Biogeosciences 11:5687–5706
Monnin C, Quéméneur M, Price R, Jeanpert J, Maurizot P, Boulart C et al (2021) The chemistry of hyperalkaline springs in serpentinizing environments: 1 the composition of free gases in New Caledonia compared to other springs worldwide. J Geophys Res Biogeosci 126:e2021JG006243
Nie NX et al (2017) Iron and oxygen isotope fractionation during iron UV photo-oxidation: implications for early Earth and Mars. EPSL 458:179–191
Okumura T, Ohara Y, Stern RJ, Yamanaka T, Onishi Y, Watanabe H et al (2016a) Brucite chimney formation and carbonate alteration at the Shinkai Seep Field, a serpentinite-hosted vent system in the southern Mariana forearc. Geochem Geophys Geosy 17:3775–3796
Okumura T, Ohara Y, Stern RJ, Yamanaka T, Onishi Y, Watanabe H, Chen C, Bloomer SH, Pujana I, Sakai S, Ishii T (2016b) Brucite chimney formation and carbonate alteration at the Shinkai Seep Field, a serpentinite-hosted vent system in the southern Mariana forearc. Geochem Geophys Geosyst 17:3775–3796
O'Neil J, Carlson R, Paquette J, Francis D (2012) Formation age and metamorphic history of the Nuvvuagittuq Greenstone Belt. Precambrian Res 220–221:23–44
Papineau D, She Z, Dodd MS, Iacoviello F, Slack JF, Hauri E, Shearting P, Little CT (2022) Metabolically diverse primordial microbial communities in Earth's oldest seafloor-hydrothermal jasper. Sci Adv 8(15):eabm2296
Pisapia C, Gérard E, Gérard M, Lecourt L, Lang SQ, Pelletier B, Payri CE, Monnin C, Guentas L, Postec A, Quéméneur M (2017) Mineralizing filamentous bacteria from the Prony bay hydrothermal field give new insights into the functioning of serpentinization-based subseafloor ecosystems. Front Microbiol 8:57
Price R, Boyd ES, Hoehler TM et al (2017) Alkaline vents and steep Na+ gradients from ridge-flank basalts—implications for the origin and evolution of life. Geology 45(12):1135–1138
Proskurowski G, Lilley MD, Seewald JS, Früh-Green GL, Olson EJ, Lupton JE et al (2008) Abiogenic hydrocarbon production at Lost City hydrothermal field. Science 319:604–607
Ranjan S, Todd ZR, Rimmer PB, Sasselov DD, Babbin AR (2019) Nitrogen oxide concentrations in natural waters on early Earth. Geochem Geophys Geosyst 20:2021–2039
Rasmussen B, Muhling JR, Fischer WW (2021) Greenalite nanoparticles in alkaline vent plumes as templates for the origin of life. Astrobiology 21:246–259
Roldan A, Hollingsworth N, Roffey A et al (2015) Bioinspired CO_2 conversion by iron sulfide catalysts under sustainable conditions. Chem Commun 51:7501–7504
Rosas JC, Korenaga J (2021) Archaean seafloors shallowed with age due to radiogenic heating in the mantle. Nat Geosci 14:51–56
Rucker HR, Kaçar B (2023) Enigmatic evolution of microbial nitrogen fixation: insights from Earth's past. Trends Microbiol
Russell MJ (2017) Life is a verb, not a noun. Geology 45(12):1143–1144
Russell MJ (2018) Green rust: the simple organizing 'seed'of all life? Life 8(3):35
Russell MJ (2023) A self-sustaining serpentinization mega-engine feeds the fougerite nanoengines implicated in the emergence of guided metabolism. Front Microbiol 14:1145915
Russell MJ, Hall AJ (1997) The emergence of life from iron monosulphide bubbles at a submarine hydrothermal redox and pH front. J Geol Soc 154:377–402
Russell MJ, Hall AJ (2006) The onset and early evolution of life, Evolution of Early Earth's Atmosphere, Hydrosphere, and Biosphere - Constraints from Ore Deposits, Stephen E. Kesler, Hiroshi Ohmoto
Sainz-Díaz CI, Escamilla-Roa E, Cartwright JHE (2018) Growth of self-assembling tubular structures of magnesium oxy/hydroxide and silicate related with seafloor hydrothermal systems driven by serpentinization. Geochem Geophys Geosyst 19:2813–2822
Stanulla R, Stanulla C, Bogason E, Pohl T, Merkel B (2017) Structural, geochemical, and mineralogical investigation of active hydrothermal fluid discharges at Strýtan hydrothermal chimney, Akureyri Bay, Eyjafjörður Region, Iceland. Geotherm Energy 5:8–18
Takahashi E, Scarfe CM (1985) Melting of peridotite to 14 GPa and the genesis of komatiite. Nature 315:566–568
Tarduno JA, Cottrell RD, Bono RK et al (2023) Hadaean to Palaeoarchaean stagnant-lid tectonics revealed by zircon magnetism. Nature 618:531–536
Templeton AS, Ellison ET (2020) Formation and loss of metastable brucite: does Fe(II)-bearing brucite support microbial activity in serpentinizing ecosystems? Phil Trans R Soc A 378(2165):20180423
Tivey MK, Singh S (1997) Nondestructive imaging of fragile sea-floor vent deposit samples. Geology 25:931–934

Tosca NJ, Guggenheim S, Pufahl PK (2016) An authigenic origin for Precambrian greenalite: implications for iron formation and the chemistry of ancient seawa-ter. Geol Soc Am Bull 128:511–530
Trolard F, Duval S, Nitschke W, Ménez B, Pisapia C, Nacib JB, Andréani M, Bourrié G (2022) Mineralogy, geochemistry and occurrences of fougerite in a modern hydrothermal system and its implications for the origin of life. Earth Sci Rev 225:103910
Twing KI, Ward LM, Kane ZK, Sanders A, Price RE, Pendleton HL, Giovannelli D, Brazelton WJ, McGlynn SE (2022) Microbial ecology of a shallow alkaline hydrothermal vent: strýtan hydrothermal field, Eyjafördur, northern Iceland. Front Microbiol 13:960335
Ueda H, Shibuya T, Sawaki Y, Shozugawa K, Makabe A, Takai K (2021) Chemical nature of hydrothermal fluids generated by serpentinization and carbonation of komatiite: implications for H2-rich hydrothermal system and ocean chemistry in the early earth. Geochem Geophys Geosyst 22(12):e2021GC009827
Von Damm KL (1990) Seafloor hydrothermal activity: black smoker chemistry and chimneys. Annu Rev Earth Planet Sci 18:173–204
Westall F, Hickman-Lewis K, Hinman N, Gautret P, Campbell KA, Bréhéret JG et al (2018) A hydrothermal-sedimentary context for the origin of life. Astrobiology 18:259–293
White LM, Bhartia R, Stucky GD et al (2015) Mackinawite and greigite in ancient alkaline hydrothermal chimneys: identifying potential key catalysts for emergent life. Earth Planet Sci Lett 430:105–114
White LM, Shibuya T, Vance SD, Christensen LE, Bhartia R, Kidd R, Hoffmann A, Stucky GD, Kanik I, Russell MJ (2020) Simulating serpentinization as it could apply to the emergence of life using the JPL hydrothermal reactor. Astrobiology 20(3):307–326
Wong ML, Charnay BD, Gao P, Yung YL, Russell MJ (2017) Nitrogen oxides in early Earth's atmosphere as electron acceptors for life's emergence. Astrobiology 17:975–983

Publisher's Note